*Remote Sens.* **2015**, *7*, 6005-6025; doi:10.3390/rs70506005

OPEN ACCESS

*remote sensing*

**ISSN 2072-4292**

www.mdpi.com/journal/remotesensing

*Article*

# A Remote Sensing Method for Estimating Surface Air Temperature and Surface Vapor Pressure on a Regional Scale

**Renhua Zhang [1], Yuan Rong [2], Jing Tian [1,3,*], Hongbo Su [1,4], Zhao-Liang Li [5] and Suhua Liu [1,6]**

[1] Key Laboratory of Water Cycle and Related Land Surface Processes, Institute of Geographical Sciences and Natural Resources Research (IGSNRR), Chinese Academy of Sciences (CAS), Beijing 100101, China; E-Mails: zhangrh@igsnrr.ac.cn (R.Z.); hongbo@ieee.org (H.S.); liulin557@163.com (S.L.)

[2] State Nuclear Electric Power Planning Design and Research Institute, Beijing 100095, China; E-Mail: rongyuanj@163.com (Y.R.)

[3] State Key Laboratory of Remote Sensing Science, Institute of Remote Sensing and Digital Earth, Chinese Academy of Sciences, Beijing 100101, China

[4] Department of Civil, Environmental and Geomatics Engineering, Florida Atlantic University, Boca Raton, FL 33431, USA

[5] Key Laboratory of Agri-informatics, Ministry of Agriculture/Institute of Agricultural Resources and Regional Planning, Chinese Academy of Sciences (CAS), Beijing 100081, China; E-Mail: lizhaoliang@caas.cn

[6] University of Chinese Academy of Sciences, Beijing 100049, China

* Author to whom correspondence should be addressed; E-Mail: tianj.04b@igsnrr.ac.cn; Tel.: +86-10-6488-9011; Fax: +86-10-6488-9169.

Academic Editors: Richard Gloaguen and Prasad S. Thenkabail

*Received: 17 March 2015 / Accepted: 5 May 2015 / Published: 13 May 2015*

---

**Abstract:** This paper presents a method of estimating regional distributions of surface air temperature ($T_a$) and surface vapor pressure ($e_a$), which uses remotely-sensed data and meteorological data as its inputs. The method takes into account the effects of both local driving force and horizontal advection on $T_a$ and $e_a$. Good correlation coefficients ($R^2$) and root mean square error (RMSE) between the measurements of $T_a/e_a$ at weather stations and $T_a/e_a$ estimates were obtained; with $R^2$ of 0.77, 0.82 and 0.80 and RMSE of 0.42K, 0.35K and 0.20K for $T_a$ and with $R^2$ of 0.85, 0.88, 0.88 and RMSE of 0.24hpa, 0.35hpa and 0.16hpa for $e_a$, respectively, for the three-day results. This result is much better than that

estimated from the inverse distance weighted method (IDW). The performance of $T_a$/$e_a$ estimates at Dongping Lake illustrated that the method proposed in the paper also has good accuracy for a heterogeneous surface. The absolute biases of $T_a$ and $e_a$ estimates at Dongping Lake from the proposed method are less than 0.5Kand 0.7hpa, respectively, while the absolute biases of them from the IDW method are more than 2K and 3hpa, respectively. Sensitivity analysis suggests that the $T_a$ estimation method presented in the paper is most sensitive to surface temperature and that the $e_a$ estimation method is most sensitive to available energy.

**Keywords:** air temperature; vapor pressure; surface energy balance; horizontal advection; regional scale

## 1. Introduction

Surface air temperature ($T_a$) and surface air vapor pressure ($e_a$), as measured at standard meteorological shelter height (about 2 m), are two primary descriptors of terrestrial environmental conditions [1]. They can not only indicate near surface atmospheric condition, but also reflect surface energy balance situations. They are the most basic parameters in the land-atmosphere system. Almost all models involving the land-atmosphere system, such as the global climate model, hydrological model, land surface model, crop growth model, weather forecasting model, *etc.*, need $T_a$ and $e_a$ as inputs. Therefore, accurate estimations of $T_a$ and $e_a$ play important roles in the study of the land-atmosphere system.

Generally, $T_a$ and $e_a$ at the field scale can be easily acquired from standard meteorological stations. However, this provides only limited information about spatial patterns over wide areas, because they are strongly affected by surface properties, which vary greatly in both time and space [1,2]. As a result, the measurements of $T_a$ and $e_a$ at meteorological stations are unrepresentative at the regional scale. For acquiring spatial distributions of $T_a$ and $e_a$, three kinds of methods were primarily used at present.

1. Geostatistical method. This method uses geostatistical models to interpolate the measurements of $T_a$ and $e_a$ obtained from meteorological stations and get the spatial maps of them. The inverse distance weighted method (IDW), the kriging interpolation method, the linear method and the spline interpolation method are the typical examples of this kind of method. The geostatistical method has been widely used by many researchers for many years [3,4]. The advantage of this kind of method is that it can be easily used on the basis of the observations of $T_a$ and $e_a$. However, because it has not considered the effects of local land surface on near-surface atmosphere through longwave radiation, heat and vapor exchange between land surface and atmosphere, the method would produce large errors when applied to a large heterogeneous surface [4,5]. Additionally, when the density of meteorological stations is sparse in the study area, the precision of the method would decrease because of the lack of observation data [1]. Furthermore, the station-based interpolation techniques suffer from the arbitrary location of weather stations [6], and different interpolation methods can produce different results [7,8].

2. Vertical lapse method. This method is often used to estimate air temperature in mountainous areas where there are large elevation variations. By assuming a specified lapse rate, typically a value, such as 6.0 or 6.5 °C/km [9], $T_a$ with adjustments for elevation is estimated according to the geolocation of the study area. Obviously, the determination of the value of the lapse rate is the key for the method. However, there are significant variations in lapse rates under different meteorological conditions and in different seasons. If the lapse rate is poorly determined, large errors of $T_a$ estimates will be produced [10].

3. Remotely-sensed land surface temperature (LST)-based method. As is well known, there is a close relationship between air temperature and land surface temperature [11]. With the developments for the ability to get spatial estimates of LST at high temporal and spatial resolution, many methods were presented to derive $T_a$ from LST. For example, some studies [12,13] use nighttime satellite LST products to estimate daily minimum $T_a$. Some studies [2,14,15] derive daily maximum $T_a$ from satellites through the vegetation index-temperature method (VI-T method), which assumes that the surface temperature of a fully-vegetated canopy equals its ambient air temperature. Shamir and Georgakakos [16] derived $T_a$ at four times using four instantaneous LST from the Moderate Resolution Imaging Spectroradiometer (MODIS). In addition, because the difference between LST and maximum $T_a$ is mainly controlled by the surface energy balance [13], some $T_a$ estimation methods based on the surface energy balance were developed. For example, Pape *et al.* [17] developed a model for simulating $T_a$ variations in high mountain landscapes at a high temporal resolution of one hour; Sun *et al.* [18] built a quantitative relationship between LST and $T_a$ based on the crop water stress index and aerodynamic resistance. Surface energy balance is a complex system depending on many environmental factors, such as solar radiation, cloud-cover, wind speed, soil moisture and land surface type [19]. Therefore, an under parameterization problem is encountered when estimating $T_a$ with this method. Additionally, the surface energy balance non-closure problem was widely observed at flux sites [20], which brings additional uncertainty to this method.

As for the estimation of $e_a$ at the regional scale, the geostatistical method is also widely used, like the estimation of $T_a$. The conventional interpolation methods include IDW, spline and kriging, Thiessen polygons and least-squares polynomial regression. Establishing an empirical function between a vapor pressure-deficient (VPD) and remotely-sensed parameter is also a common method of estimating $e_a$. For example, Granger [21] modelled VPD as a function of saturated vapor pressure ($e_s$) and the long-term average of $T_a$. Hashimoto *et al.* [22] estimated the spatial distribution of VPD with a simple linear relationship between it and LST retrieved from MODIS. With the availability of satellite total precipitable water (TPW) products, some studies have used TPW to estimate $e_a$ by establishing the regression functions between TPW and $e_a$ or air-specific humidity, such as the approaches presented by Sobrino *et al.* [23] and Recondo *et al.* [24]. However, the relationship between TPW and $e_a$ is empirical, which can only apply to the specific area by the limitation of the training dataset.

As stated above, most approaches for estimating $T_a$ and $e_a$ at present are based on statistical or empirical methods. In physics, two forces control $T_a$ and $e_a$. One is the turbulent flow exchange, including vertical turbulent diffusion/exchange and horizontal advection. The other is the radiation effect, which mainly indicates the heating effect of surface longwave radiation on near-surface atmosphere. Vertical turbulent diffusion/exchange and the radiation effect are primarily determined by

the local meteorological conditions and surface properties. However, horizontal advection is mainly related to the environmental and meteorological conditions at the regional scale. On a windy day, horizontal advection may play a greater role with respect to air temperature and vapor pressure; while in calm weather, local environmental conditions may dominate $T_a$ and $e_a$ by the influence of the radiation effect and vertical turbulent diffusion/exchange.

The objective of this paper is to develop a method that takes into account the effects of both local driving forces and horizontal advection on the near-surface atmosphere, for estimating regional distributions of $T_a$ and $e_a$. For a clear description, the method for air temperature is called advection-energy balance for air temperature (ADEBAT), and the method for vapor pressure is called advection-energy balance for air water vapor pressure (ADEBAV) in the paper. Section 2 describes the derivations of the ADEBAT method and the ADEBAV method. The study area and the data are introduced in Section 3. Section 4 provides the results of the $T_a$ and $e_a$ estimates. The conclusions are given in Section 5.

## 2. Methodology

### *2.1. The Derivation of the ADEBAT Method*

At the field scale, two local physical processes result in $T_a$: (1) the heating effect of land surface longwave radiation on near-surface air; in the daytime, LST is usually higher than $T_a$, because of the strong surface absorption of solar radiation; in this condition, $T_a$ increases by absorbing surface longwave radiation; (2) the effect of vertical turbulent flow, meaning the vertical heat exchange between surface and near-surface atmosphere. The two processes illustrate the reason why there is a very close relationship between LST and $T_a$. In the paper, the two processes are called the local driving force of $T_a$.

Neglecting systematic sampling errors, systematic instrument bias, low and high frequency loss of turbulent fluxes and energy sinks, horizontal advection of heat and water vapor is regarded as the primary reason for the non-closure of the surface energy balance [20,25,26]. When the effects of the factors mentioned above on the surface energy balance closure are neglected and in a situation in which there is no horizontal advection, the surface energy budget is balanced, namely surface energy balance closure. In this case, $T_a$ is dominated by local driving force and can be derived as Equation (4) according to the surface energy balance equation (Equation (1)), the heat diffusion equation (Equation (2)) and the definition of the Bowen ratio (Equation (3)).

$$R_n = H + LE + G \tag{1}$$

$$\mathrm{H} = \frac{\rho Cp}{r_a}(T_0 - T_a) \tag{2}$$

$$\beta = \frac{H}{LE} \tag{3}$$

$$T_a = T_0 - \left[\frac{\beta(R_n - G)}{(\beta + 1)}\frac{r_a}{\rho Cp}\right] \tag{4}$$

where $R_n$ is the net radiation. H and LE are sensible heat flux and latent heat flux, respectively. G is soil heat flux. $r_a$ is aerodynamic resistance. $\rho$Cp is the volumetric heat capacity of air. $T_0$ is aerodynamic temperature and is usually replaced by LST in applications [27,28]. $\beta$ is the Bowen ratio.

On the contrary, under the condition that there is obvious horizontal advection, like in windy weather, horizontal movement of the air mass would have a great influence on $T_a$. In this case, similar $T_a$ would be observed at a regional scale, and the local driving force becomes less dominant. In practice, the surface energy balance is not closed in most cases [20], which means both the local driving force and horizontal advection have influences on $T_a$.

For a constant air column in a closed system, its temperature is mainly determined by the available energy ($R_n$−G), meteorological conditions and surface properties. When there is air from outside coming into the closed system, the air temperature would be changed through air mixing. When the air temperature outside is higher than that in the closed system, $T_a$ in the closed system would increase. Conversely, it would decrease. This kind of effect of exotic air on $T_a$ is like the effect of the horizontal advection. Assuming that the inner and the exotic effects on $T_a$ agree with the linear mixture theory and using $V_{awl}$ and $V_{ajd}$ to express the air volume coming into the closed system from outside and the original air volume in the closed system, respectively, Equations (5) and (6) were established.

$$T_{azs} = fT_{awl} + (1 - f)T_{ajd} \tag{5}$$

$$\mathrm{f} = \frac{V_{awl}}{V_{azs}} \ (1 - \mathrm{f}) = \frac{V_{ajd}}{V_{azs}} \tag{6}$$

where $V_{azs}$ is the total air volume and equals the sum of $V_{awl}$ and $V_{ajd}$. $T_{azs}$ is the final air temperature. In practice, it is the real air temperature observed at the meteorological station. $T_{awl}$ is the air temperature affected by horizontal advection. $T_{ajd}$ is the original air temperature in the closed system, which is the air temperature under the condition of surface energy balance closure and is controlled by the local driving force. $f$ is the volume percentage, ranging from 0 to 1, which represents the weight of the effects of horizontal advection on $T_{azs}$. From Equation (5), it can be seen that $f = 0$ means there is no horizontal advection (surface energy balance closure), and $T_{azs}$ is totally controlled by the local driving force; while $f = 1$ means that there is no local driving force and that $T_{azs}$ is totally controlled by horizontal advection. In most cases, $f$ is between 0 and 1.

Estimating $T_{azs}$ is the purpose of this paper. Obviously, three parameters of $f$, $T_{awl}$ and $T_{ajd}$ must be calculated first to estimate $T_{azs}$.

#### 2.1.1. The Calculation of $T_{ajd}$

The surface energy balance equation describes the relationship between surface energy components well under the condition of surface energy balance closure. On the basis of this, $T_a$ under the condition of surface energy balance closure can be derived as Equation (4). Therefore, $T_{ajd}$ can be calculated from Equation (4) in which $T_a$ is $T_{ajd}$.

For calculating $T_{ajd}$, $r_a$ in the condition of no horizontal advection needs to be determined. In the study, a value of $r_a$ of 65 s/m, which is determined by a lab experiment, was used to compute $T_{ajd}$. In the experiment, radiometric soil surface temperature ($T_s$), $e_a$ and evapotranspiration for bare soil with saturated soil water content were measured in a no-wind condition. Then, $r_a$ was retrieved in terms of Equation (7).

$$\mathrm{LE} = \frac{\rho C_p}{\gamma(r_a + r_s)}(e_s - e_a) \tag{7}$$

where $e_s$ is surface saturated vapor pressure, which is calculated by Equation (8). $r_s$ is surface resistance and equals zero for soil with saturated soil water content; $\gamma$ is the psychrometer constant.

$$e_s = 6.108 \times \exp(\frac{17.27T_0}{T_0 + 237.3}) \quad (8)$$

where $T_0$ is aerodynamic temperature. In the study, $T_0$ is replaced by $T_s$ [29,30].

An empirical method presented by Zhang *et al.* [31] was used to estimate $\beta$.

$$\beta = A\frac{(P_{max} - P_{min}) - (P_i - P_{min})}{(P_i - P_{min})} \quad (9)$$

where A is an empirical coefficient and equals 0.66 according to the literature. P is a simplified thermal inertia defined as:

$$P = \frac{\overline{Rn}((t_2 - t_1))^{0.5}}{(T_{02} - T_{01})} \quad (10)$$

$T_{02}$ is the surface temperature at satellite overpass time. $T_{01}$ is the daily minimum surface temperature usually occurring at the time before sunrise. $t_2$ and $t_1$ are the times when $T_{02}$ and $T_{01}$ occur. $\overline{Rn}$ is the average net radiation from $t_1$ to $t_2$. $P_{max}$ and $P_{min}$ are the maximum and the minimum thermal inertia, respectively, for a given fractional vegetation cover ($f_v$), which are determined by the trapezoid space formed by the scatter plot of remotely-sensed vegetation index (VI) *versus* LST.

$R_n$ and G were estimated by Equations (11) and (12).

$$R_n = S_0(1 - \alpha) + R_{ld} - \sigma\varepsilon T_0^4 \quad (11)$$

$$G = 0.3(1 - 0.9f_v)R_n \quad (12)$$

where $\sigma$ is the Stefan–Boltzmann constant. $\alpha$ is surface albedo. $\varepsilon$ is surface emissivity. $R_{ld}$ is downward longwave radiation.

### 2.1.2. The Calculation of *f* and $T_{awl}$

In the study, meteorological measurements of air temperature, wind speed and wind direction at weather stations were used to calculate $f_i$ and $T_{iawl}$. $i$ represents the pixel at which air temperature is to be estimated. The procedures of estimating them at pixel $i$ are:

1. Selecting two weather stations nearest to pixel $i$. The two stations must have similar wind speed and wind direction. Here, similar wind speed and wind direction is assumed to have similar horizontal advection. The pixels at which the two weather stations are located are represented as Pixel 1 and Pixel 2. Under the assumption that horizontal advection is the same over a regional area, the horizontal advection at pixel $i$ is the same as that at Pixel 1 and Pixel 2. As a result, $T_{1awl} = T_{2awl} = T_{iawl}$, $f_1 = f_2 = f_i$.
2. Calculating the $T_{ajd}$ map with Equation (4) based on $r_a$ and the remotely-sensed data of $R_n$, G and LST;
3. At Pixel 1 and Pixel 2, the following two equations can be established based on Equation (5):

$$T_{1azs} = f_1T_{1awl} + (1 - f_1)T_{1ajd} \quad (13)$$

$$T_{2azs} = f_2T_{2awl} + (1 - f_2)T_{2ajd} \quad (14)$$

$T_{1azs}$ and $T_{2azs}$ are the observed air temperatures at Pixel 1 and Pixel 2. $T_{1ajd}$ and $T_{2ajd}$ are the air temperatures affected by the local driving force at Pixel 1 and Pixel 2, which is obtained from Step (2). Because $T_{1awl} = T_{2awl} = T_{iawl}$, $f_1 = f_2 = f_i$, $f$ and $T_{awl}$ at pixel $i$ can be estimated from Equations (13) and (14).

$$f_i = 1 - \frac{T_{1azs} - T_{2azs}}{T_{1ajd} - T_{2ajd}} \tag{15}$$

$$T_{iawl} = \frac{(T_{1azs} + T_{2azs}) - (1 - f_i)(T_{1ajd} + T_{2ajd})}{f_i} \tag{16}$$

Integration of Equations (15) and (16) into Equation (5) and combining $T_{ajd}$ results from Step (2); $T_{azs}$ at pixel $i$ is calculated.

### *2.2. The Derivation of the ADEBAV Method*

The idea of the method of estimating air vapor pressure is similar to that of air temperature. The local driving force and horizontal advection are also the primary factors influencing near-surface vapor pressure. When there is no horizontal advection, $e_a$ under the condition of surface energy closure can be estimated from Equation (17), which is deduced from Equations (1), (3) and (7).

$$e_a = e_s - \left[\frac{(R_n - G)\gamma(r_a + r_s)}{\rho Cp(\beta + 1)}\right] \tag{17}$$

The parameters have the same meanings with the above descriptions.

Under the condition that there are both effects of the local driving force and horizontal advection, $e_a$ can be expressed as Equation (19) in terms of the linear mixture theory.

$$e_{azs} = f e_{awl} + (1 - f) e_{ajd} \tag{18}$$

where $e_{azs}$ is the real vapor pressure and $e_{awl}$, $e_{ajd}$ are the vapor pressures affected by horizontal advection and the local driving force, respectively.

Equation (17) gives the estimation of vapor pressure under the condition of surface energy balance closure, so $e_{ajd}$ can be calculated from it in which $e_a$ is $e_{ajd}$. The methods of calculating $R_n$, G, $\beta$ and $r_a$ are the same as that used in calculating $T_{ajd}$; see Section 2.1.1. The VI-T trapezoid method was used to acquire $r_s$ [32], which is formed by the scatter plot of VI *versus* T under a full range of vegetation cover and soil moisture availability and has been widely used to infer soil moisture and to quantify land surface evaporation [33–36]. In the trapezoid method, the dry edge is the uppermost line of the VI-T space, the pixels on which are taken as surfaces with the largest water stress (soil water content reaches wilting point), and thereby, $r_s$ is largest on the dry edge. The wet edge is the lowest line of the VI-T space, the pixels that represent surfaces without water stress, and thereby, $r_s$ is smallest on the wet edge. An isopleth line within the trapezoid space has the same soil surface moisture availability. According to this, $r_s$ for every pixel was interpolated in terms of the LST difference between the pixel and the dry edge and the LST difference between the pixel and the wet edge; see Equation (18).

$$r_s = \frac{T - T_{min}}{T_{max} - T_{min}}(r_{s\_max} - r_{s\_min}) \tag{19}$$

where $T_{max}$ and $T_{min}$ are the corresponding maximum and minimum surface temperatures at the dry and wet edges, respectively, for a given $f_v$. $r_{s\_max}$ and $r_{s\_min}$ are the maximum and minimum surface resistance,

respectively. $r_{s\_min}$ equals zero when the soil water content is saturated. For sandy loam, which is the dominant soil type in the North China Plain (the study area in the paper), the wilting point at a depth of 0–20 cm is about 0.07 v/v, and the saturated water content at a depth of 0–20 cm is about 0.3 v/v [37,38]. According to the studies of Camillo [39] and Sun [40], $r_{s\_max}$ for sandy loam was set as 140 s/m in the study when soil water content reached the wilting point.

The procedures of the calculation of *f* and $e_{awl}$ for pixel *i* are the same as that in calculating $T_{awl}$; see Section 2.1.2. Air temperature is replaced by vapor pressure. The formulas of *f* and $e_{awl}$ for pixel *i* are:

$$f_i = 1 - \frac{e_{1azs} - e_{2azs}}{e_{1ajd} - e_{2ajd}} \tag{20}$$

$$e_{iawl} = \frac{(e_{1azs} + e_{2azs}) - (1 - f_i)(e_{1ajd} + e_{2ajd})}{f_i} \tag{21}$$

where the subscripts of 1 and 2 represent the two selected weather stations determined by Step (1). Integrating Equations (20) and (21) into Equation (19) and combining the calculated $e_{ajd}$, $e_{azs}$ for pixel *i* is estimated.

It should be noted that $T_a$ and $e_a$ estimated with this method are the air temperature and the water vapor pressure instantaneously at the satellite overpass time, because remotely-sensed data of $R_n$, G and LST are the important inputs of the method, which can only represent the values at the satellite overpass time.

## 3. The Study Area and the Dataset

The study area is located in the North China Plain and ranges from 35.0°N to 38.3°N in latitude, from 116.0°E to 118.5°E in longitude. The land use in the area is dominated by the rotating cropping of winter wheat and summer maize. Millet, soybean and cotton are also scatter planted in summer. According to the traditional tillage practice, winter wheat is sown in early October, harvested in early or mid-June next year, and summer maize is planted in early to mid-June and harvested at the end of September. The soil types are mostly sandy loam. Annual precipitation is about 600 mm, more than 50% of which falls during the summer monsoon between July and September. The groundwater table varies from 1.5 m to 3.5 m with an average of 2.5 m.

In the study, field measurements at 40 standard meteorological stations were used, shown in Figure 1. The measurements include air temperature, vapor pressure, wind speed, wind direction and solar radiation at about a 2-m height above the surface at 2:00, 8:00, 14:00, 20:00. $T_a$, $e_a$ and solar radiation at the satellite overpass time are obtained by a linear interpolation. The measurements from about 20 stations were used to calculate *f* and $T_{awl}$/$e_{awl}$. The measurements at the other stations were used to validate the estimates of $T_a$ and $e_a$. The triangle symbol in Figure 1 is Dongping Lake. The circle on the upper right corner is a water area close to Bohai Gulf.

Considering that the effect of the local driving force on near-surface atmosphere is only obvious within a small area, Landsat TM data with a high spatial resolution of 120 m in the infrared wave band were used in the study to estimate regional $T_a$ and $e_a$. The overpass time of Landsat TM in the study area is at about 10:40 local time. The single-window method presented by Qin *et al.* [41] was used to retrieve LST in the daytime. Surface albedo was retrieved by Liang's method [42].

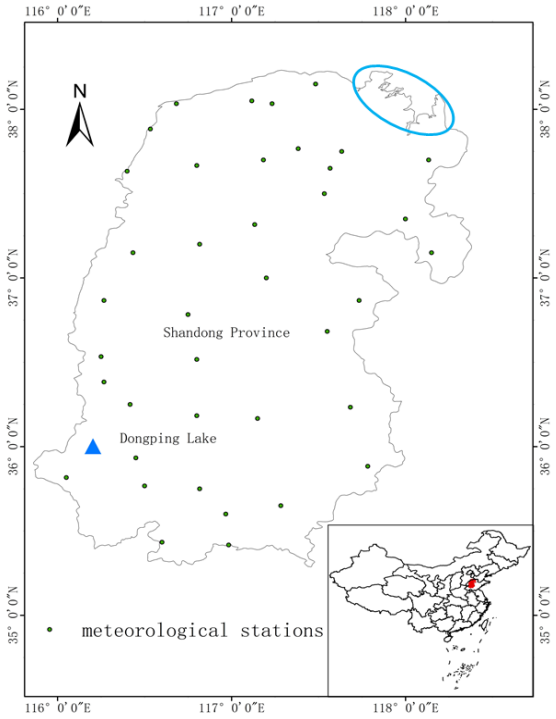


**Figure 1.** Study area and the distribution of the weather stations.

To acquire the daily minimum surface temperature, the Chinese geostationary Fengyun Meteorological satellite (FY-2C) data were used. FY-2C, developed by Shanghai Academy of Space Flight Technology and China Academy of Space Technology and operated by China Meteorological Administration (CMA), was launched on 19 October 2004 and has been fully operational since 2006. It is located above the Equator at longitude 105°E and about 35,800 km above the ground, and it can acquire one full disc image covering the Earth surface from 60°N to 60°S in latitude and from 45°E to 165°E in longitude per hour and 30 min per acquisition for flood seasons (usually from 1 June to 31 August). The imaging radiometer consists of one visible channel and four infrared channels. A surface temperature inversion method corresponding to FY-2C [43] was used to retrieve FY-2C LST at the time before sunrise. A bilinear interpolation method was used to downscale the FY-2C LST from 5 km to 120 m to match the spatial resolution of Landsat TM. Table 1 lists the variables and the sources used in the study.

**Table 1.** Variables and the sources used in the study. FY-2C, Fengyun Meteorological satellite.

| Variables | Sources | Resolution |
|---|---|---|
| LST in the daytime | Landsat TM | 120 m |
| LST at the time before sunrise | FY-2C | downscaled from 5 km to 120 m |
| Net radiation | Landsat TM | 120 m |
| Soil heat flux | Landsat TM | 120 m |
| Solar radiation, wind speed, air temperature, water vapor pressure | Meteorological stations | |

In the study, three clear-sky days on 8 April, 30 August and 17 October in 2009 were selected to perform the calculations. The sunrise times for the 3 days are at 6:49, 5:42 and 6:23 local time,

respectively, so FY-2C data with the acquisition time closest to the sunrise for the 3 days were used to obtain the daily minimum surface temperatures.

For evaluating the methods, the IDW method was also used to estimate $T_a$ and $e_a$. The same stations used in the methods of ADEBAT and ADEBAV were used to perform the IDW interpolation and the validations. The two sets of estimates of $T_a/e_a$ obtained from the IDW method, the ADEBAT method and the ADEBAV method, respectively, were compared.

## 4. Results

### *4.1. Air Temperature Retrievals by the ADEBAT Method and Its Validation*

The comparisons between $T_a$ estimated from the ADEBAT method and the IDW method and the measurements for the three days are given in Figure 2, respectively. It shows that the correlation coefficient ($R^2$) for the ADEBAT method, with $R^2$ of 0.77, 0.82 and 0.80, respectively, for the three days, is obviously higher than that for the IDW method, with $R^2$ of 0.3, 0.50 and 0.25. The root mean square error (RMSE) for the ADEBAT method, with RMSE of 0.42K, 0.35K and 0.20K, respectively, for the three days, is smaller than that for the IDW method, with RMSE of 0.82K, 0.39K and 0.65K. Figure 2 also shows that $T_a$ estimates from the ADEBAT method are closer to the 1:1 line than those from the IDW method. This illustrates that the accuracy of the $T_a$ estimation based on the ADEBAT method is obviously higher than that based on the IDW method.

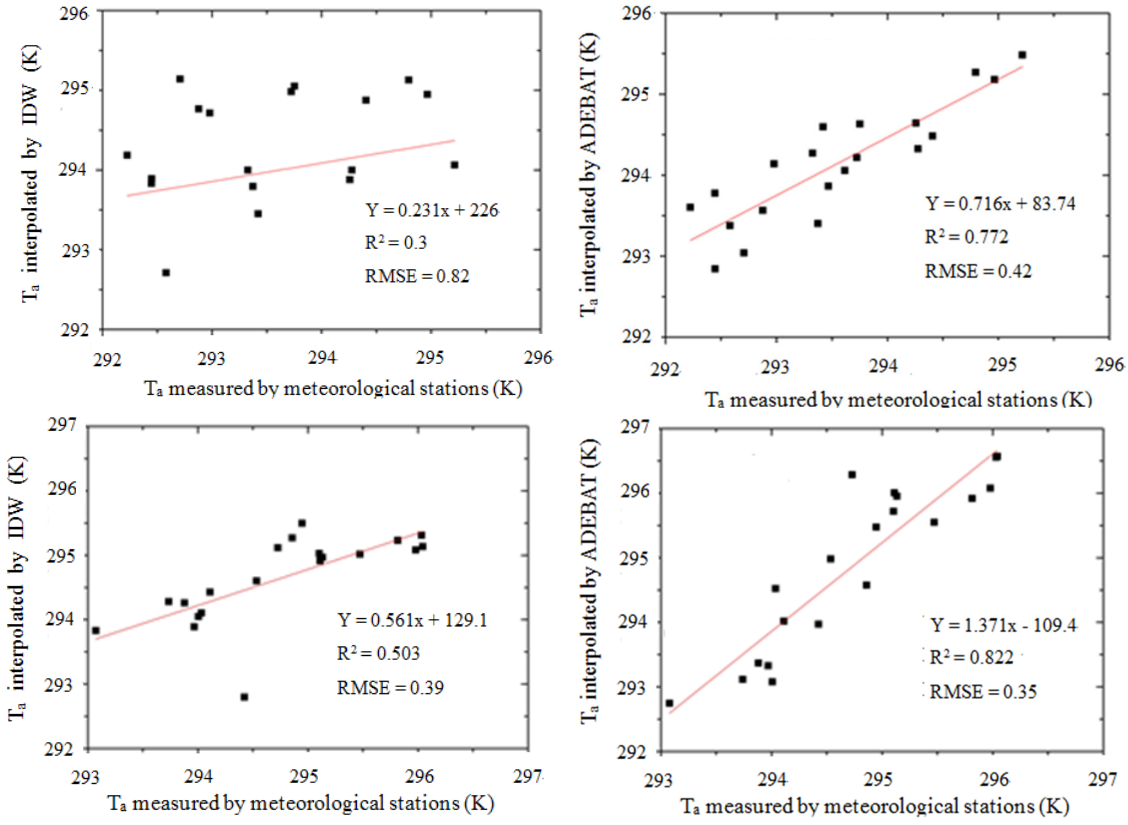


**Figure 2.** *Cont.*

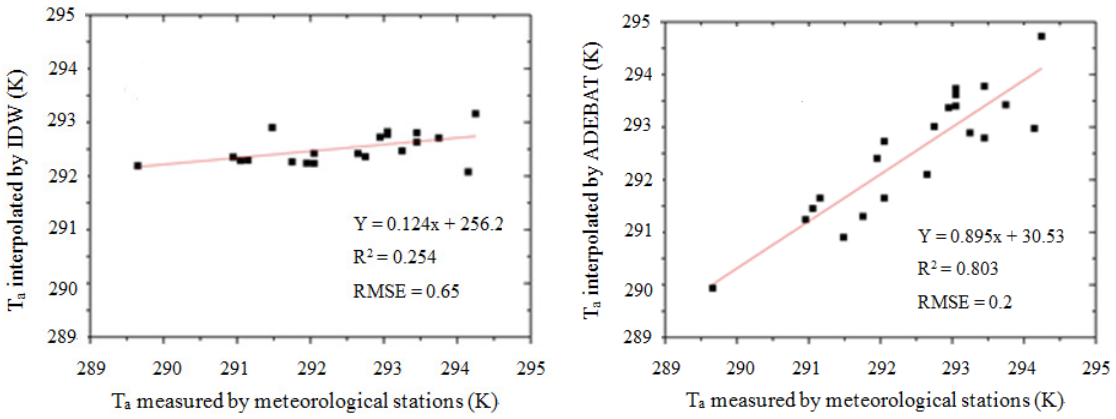


**Figure 2.** Comparisons between $T_a$ measurements and $T_a$ estimates from the inverse distance weighted (IDW) method (**left**) and the advection-energy balance for air temperature (ADEBAT) method (**right**) on 8 April, 30 August and 17 October in 2009.

Compared with the geostatistical interpolation methods, like the IDW method, the ADEBAT method takes into account the effects of not only horizontal advection, but also the local driving force on near-surface atmosphere, while the IDW method only considers some effects of horizontal advection by calculating the distance of the pixel to be interpolated to the weather station. In other words, it does not consider any information about the effects of the local driving force on $T_a$. When there is a relatively uniform surface within the study area, which means the effects of the local surface condition on near-surface atmosphere are similar over the area, or there is strong horizontal advection when the local condition has few effects, like in windy weather, the geostatistical interpolation method may be proper. However, when the local surface condition dominates $T_a$, the geostatistical interpolation method would produce large errors. In this case, the ADEBAT method would have a great advantage over the IDW method.

Taking $T_a$ estimates at Dongping Lake as an example, the advantage of the ADEBAT method over the geostatistical method was illustrated further. Dongping Lake is located in Doping county of Shandong province (see Figure 1), which covers an area of 124.3 $km^2$. The average water depth is 2.5 m. This large water body could have a great effect on the near-surface atmosphere over it, so $T_a$ over the lake and over the land should have a large difference. Table 2 lists the comparisons between the estimated $T_a$ by the IDW method and the ADEBAT method and the $T_a$ measurements at Dongping Lake. It can be seen that the absolute bias (AB) between the estimates and the observations for the ADEBAT method is much smaller than that for the IDW method. AB for the ADEBAT method is less than 0.5K, while AB for the IDW method is more than 2K. Table 2 also gives the $T_a$ measurements at the two selected stations (Station 1 and Station 2) used to calculate $f$ and $T_{awl}$ at Dongping Lake in the ADEBAT method. There are large differences in $T_a$ between the two stations, with a grassland underlying surface, and Dongping Lake, due to the large difference of land surface type. Because the ADEBAT method takes into account the effect of the local driving force on $T_a$, the estimated $T_a$ at Dongping Lake is still very close to the observations.

Therefore, the ADEBAT method is better than the IDW method, especially for an area with a large heterogeneous surface, in which case the effect of the local driving force on near-surface atmosphere may have a large difference.

**Table 2.** Comparisons between the estimated air temperatures by the IDW method and the ADEBAT method and the $T_a$ measurements at Dongping Lake (K).

| | $T_a$ at Station 1 | $T_a$ at Station 2 | $T_a$ Estimates From the IDW Method | $T_a$ Estimates From the ADEBAT Method | $T_a$ Measurements | Absolute Biases for the IDW Method | Absolute Biases for the ADEBAT Method |
|---|---|---|---|---|---|---|---|
| 8 April | 294.95 | 294.62 | 294.76 | 290.24 | 290.43 | 4.33 | 0.19 |
| 30 August | 294.87 | 295.55 | 295.23 | 292.45 | 292.87 | 2.36 | 0.42 |
| 17 October | 293.25 | 293.65 | 293.56 | 289.88 | 290.23 | 3.33 | 0.35 |

### *4.2. Vapor Pressure Retrievals by the ADEBAV Method and Its Validation*

Figure 3 displays the scatter plots of $e_a$ estimates and $e_a$ measurements for the three days for the IDW method and the ADEBAV method, respectively. Compared with the $e_a$ estimates based on the IDW method, the results estimated by the ADEBAV method are much better. Clearly, the ADEBAV method obtained better values of $R^2$ and RMSE. For the ADEBAV method, the values of $R^2$ are 0.85, 0.88 and 0.88 and the RMSE values are 0.24hpa, 0.35hpa and 0.16hpa, respectively, for the three days; while for the IDW method, the $R^2$ values are only 0.22, 0.33 and 0.03 and the RMSE values are 1.45hpa, 0.96hpa and 0.45hpa. Figure 3 also shows that the $e_a$ estimates from the ADEBAT method are closer to the 1:1 line than those from the IDW method.

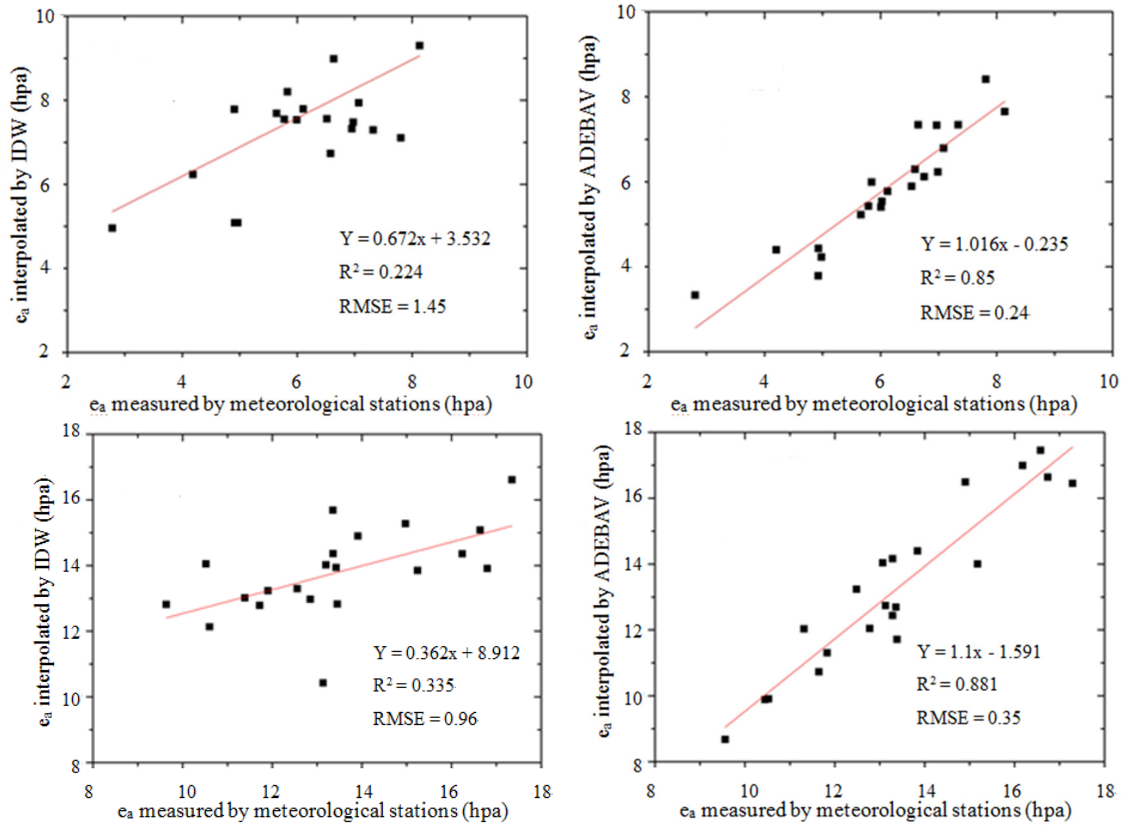


**Figure 3.** *Cont.*

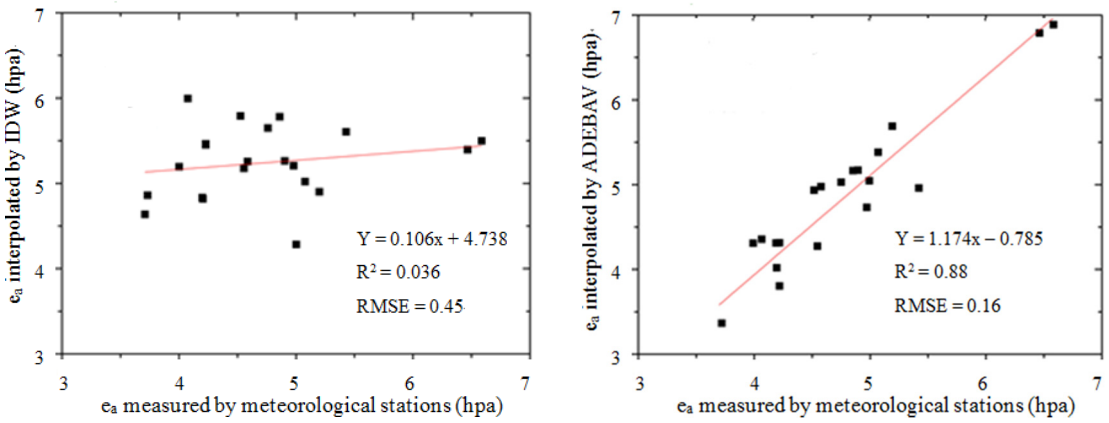


**Figure 3.** Comparisons between $e_a$ measurements and $e_a$ estimates from the IDW method (**left**) and the ADEBAT method (**right**) on 8 April, 30 August and 17 October in 2009

Table 3 gives the $e_a$ estimates by the IDW method and the ADEBAV method and the measurements at Dongping Lake. Smaller AB for $e_a$ of 0.5, 0.7 and 0.6hpa for the three days for the ADEBAV method were obtained. Comparatively, AB for the IDW method is five- to 10-times as much as that for the ADEBAV method, reaching 4.87, 3.78 and 5.13hpa for the three days. Lack of consideration for the local driving force on $e_a$ in the IDW method is the main reason for this.

**Table 3.** Comparisons between the estimated vapor pressure by the IDW method and the ADEBAT method and the $e_a$ measurements at Dongping Lake (hpa). ADEBAV, advection-energy balance for air water vapor pressure.

| Date | $e_a$ at Station 1 | $e_a$ at Station 2 | $e_a$ Estimates from the IDW Method | $e_a$ Estimates from the ADEBAT Method | $e_a$ Measurements | Absolute Biases for the IDW Method | Absolute Biases for the ADEBAV Method |
|---|---|---|---|---|---|---|---|
| 8 April | 7.8 | 6.74 | 7.43 | 12.8 | 12.3 | 4.87 | 0.5 |
| 30 August | 16.8 | 13.91 | 15.42 | 19.9 | 19.2 | 3.78 | 0.7 |
| 17 October | 5.8 | 5.36 | 5.67 | 10.2 | 10.8 | 5.13 | 0.6 |

### *4.3. Comparisons of the Spatial Distributions of $T_a$ and $e_a$*

Figures 4 and 5 show the spatial distributions of $T_a$ estimates and $e_a$ estimates by the IDW method and the ADEBAT/ADEBAV method. It can be seen that the distributions of $T_a$ estimates and $e_a$ estimates exhibit an obvious circular spatial pattern for the IDW method. It centers on several areas and radiates out from these centers with a gradient trend form. This kind of spatial pattern actually does not exist in nature.

Limited by the algorithm of the IDW method, the maximum and the minimum $T_a$ or $e_a$ in the study area are completely determined by the maximum and the minimum $T_a$ or $e_a$ observations at weather stations. Because the IDW method totally depends on the number and the spatial distributions of the weather stations and the $T_a$/$e_a$ measurements at the weather stations, these unreasonable phenomena were produced.

Comparatively, the results based on the ADEBAT/ADEBAV method provide more details about the spatial patterns of $T_a$ and $e_a$. At Dongping Lake, no differences in the estimates of $T_a$ and $e_a$ between the

lake and the land were obtained for the IDW method. In addition, $T_a/e_a$ estimates from the ADEBAT/ADEBAV method display large differences between the lake and the land. $T_a$ over the lake is obviously lower than that over the land, and $e_a$ over the lake is obviously higher than that over the land. Lower $T_a$ estimates and higher $e_a$ estimates were also obtained over the water area close to Bohai Gulf. The performance of $T_a$ and $e_a$ estimates at the water surface suggests that the result obtained from the ADEBAT/ADEBAV method is more reasonable than that from the IDW method.

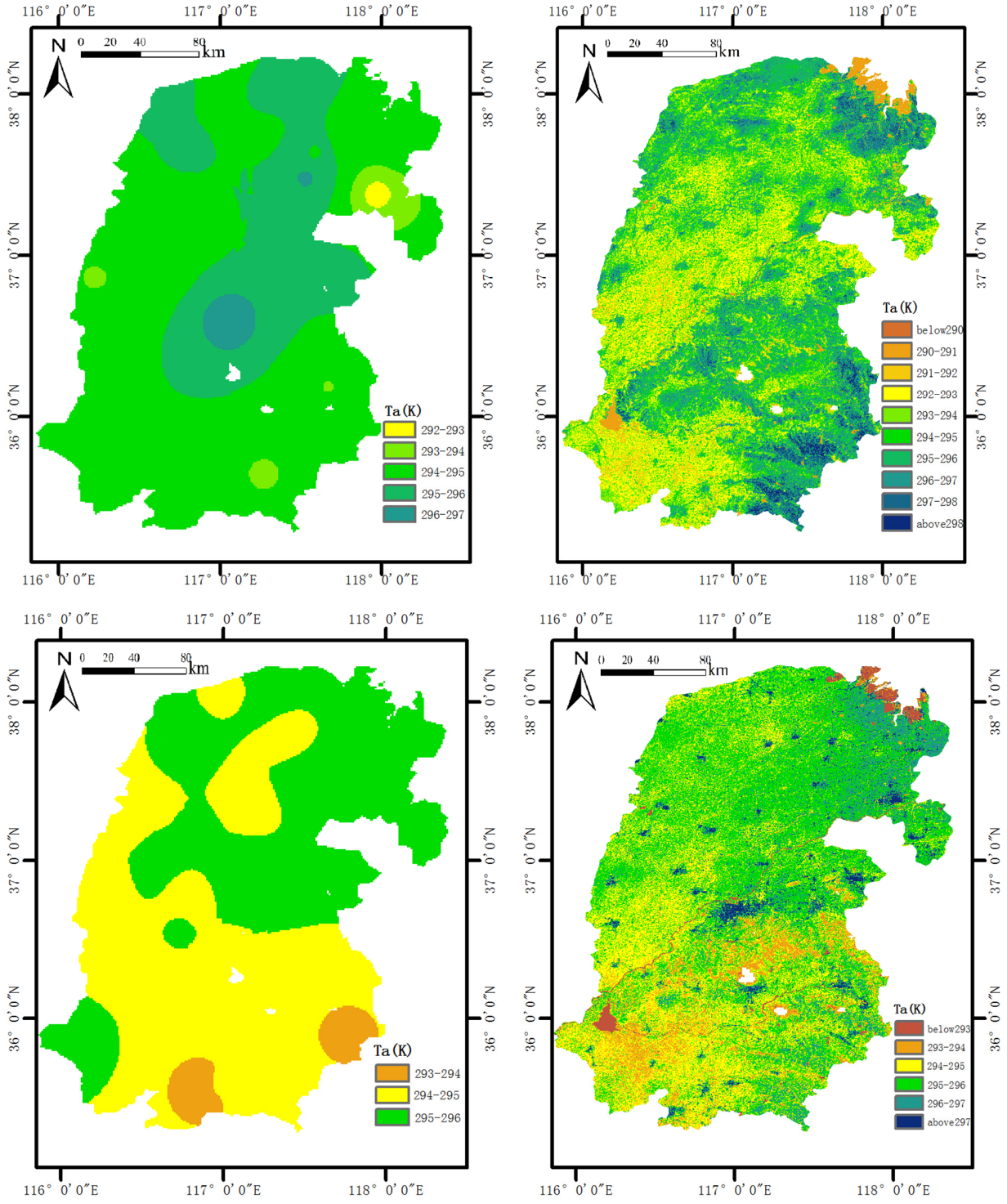


**Figure 4.** *Cont.*

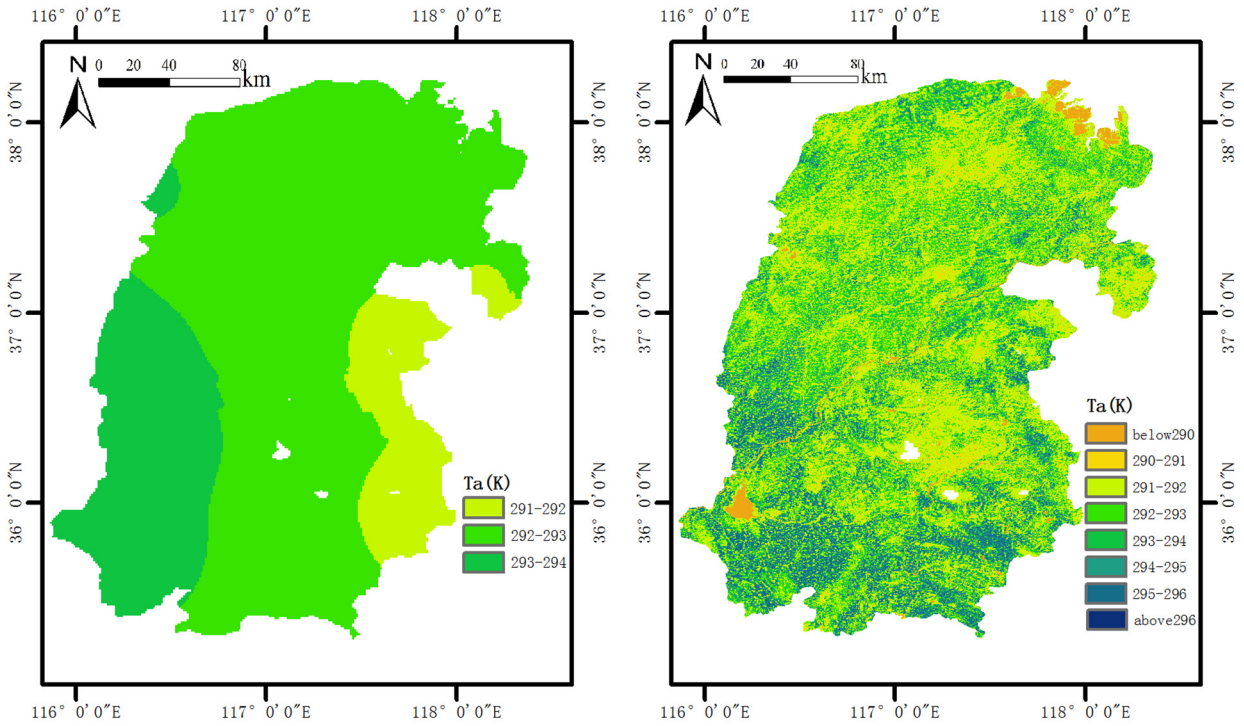


**Figure 4.** Spatial distributions of $T_a$ estimates from the IDW method (**left**) and the ADEBAT method (**right**) on 8 April, 30 August and 17 October in 2009.

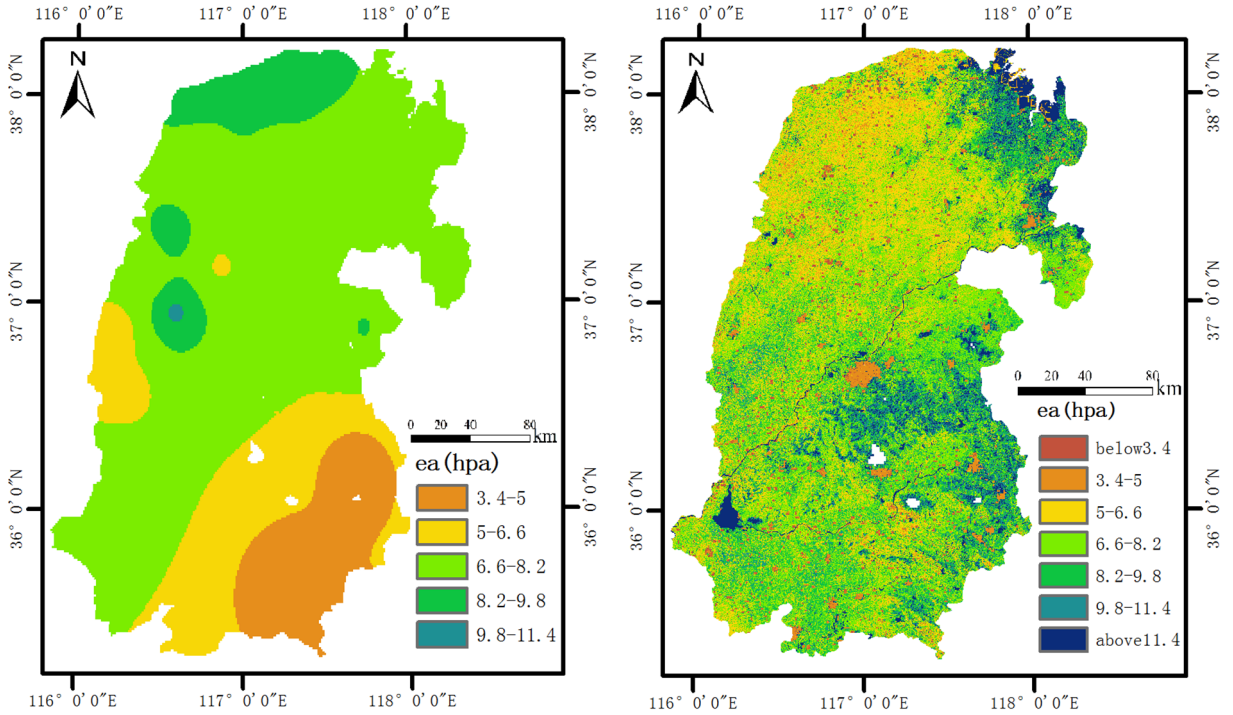


**Figure 5.** *Cont.*

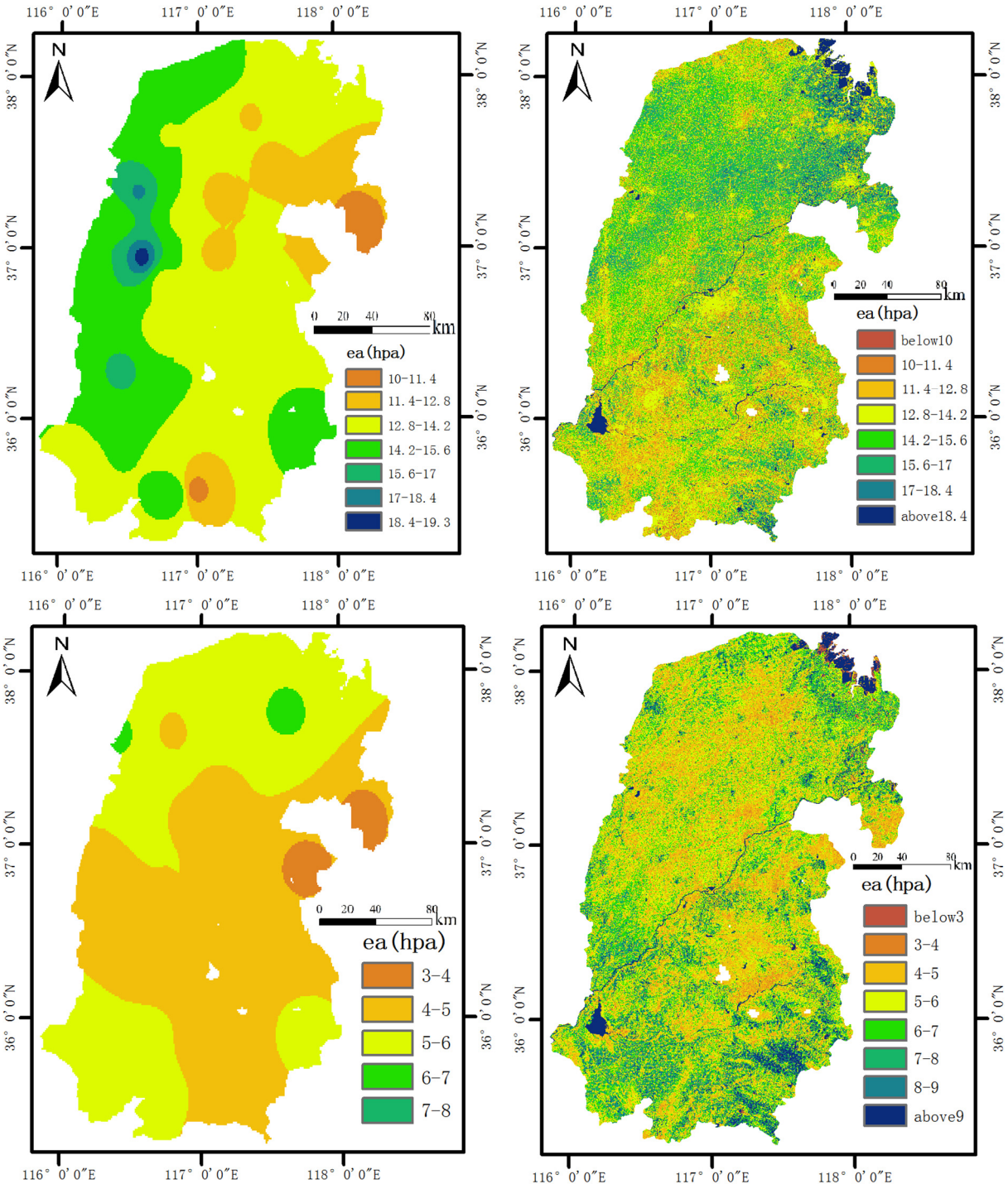


**Figure 5.** Spatial distributions of $e_a$ estimates from the IDW method (**left**) and the ADEBAV method (**right**) on 8April, 30 August and 17 October in 2009.

## 5. Sensitivity Analysis

Sensitivity analysis plays a fundamental role in understanding the contributions of variables and parameters to model output. In this study, the sensitivity of $T_a$ to the inputs of $T_0$, $R_n$−G, $r_a$ and $\beta$ for the ADEBAT method and the sensitivity of $e_a$ to the inputs of $T_0$, $T_a$ (used to calculate $e_s$), $R_n$−G, $r_a$, $r_s$ and $\beta$ for the ADEBAV method were analyzed, respectively. Perturbations of $T_0$ and $T_a$ were specified as

[−2K, 2K], with a variation step of 1K. Perturbations of $R_n$−G, $\beta$, $r_a$ and $r_s$ were specified as [−20%, 20%], with a variation step of 10%.

Results (Table 4) show that for the ADEBAT method, $r_a$, $R_n$−G and $\beta$ are negatively correlated with $T_a$, but $T_0$ is positively correlated with $T_a$. Comparing the sensitivity of $T_a$ to the four inputs, $T_a$ is most sensitive to $T_0$. A 1K increase of $T_0$ could result in a 0.6K increase in $T_a$ estimates. A similar sensitivity of $T_a$ to $r_a$ and $R_n$−G was observed. A 10% increase of $r_a$ or $R_n$−G could result in a 0.35K decrease in $T_a$ estimates. The sensitivity of $T_a$ to $\beta$ is the least. A 10% variation of $\beta$ only produces about a 0.24K variation of $T_a$.

For the ADEBAV method (Table 5), $r_a$, $r_s$ and $R_n$−G are all negatively correlated with $e_a$ estimates. $T_a$ and $\beta$ are positively correlated with $e_a$ estimates. The order of the sensitivities of $e_a$ to the five inputs from the most to the least is $R_n$−G, $r_s$, $r_a$, $\beta$ and $T_a$, respectively. A 10% increase of $R_n$−G could result in a 0.37-hpa decrease of $e_a$ estimates. A 10% increase of $r_a$ or $r_s$ could produce about a 0.23-hpa decrease in $e_a$ estimates. A 10% variation of $\beta$ produces about a 0.2-hpa variation of $T_a$. A 1K increase of $T_a$ only produces a 0.1-hpa increase in $e_a$ estimates.

In application, the calculation of $\beta$ has more uncertainty. However, the good thing is that the ADEBAT method and the ADEBAV method are not very sensitive to $\beta$ according to the sensitivity analysis. There is still some uncertainty about the determinations of $r_a$ and $r_s$, which are difficult to estimate precisely. Fortunately, the ADEBAT method and the ADEBAV method are not very sensitive to them.

**Table 4.** The sensitivity of $T_a$ estimates from the ADEBAT method to each input variable. Variations of $T_0$ are in K, and variations of other variables are a percentage (%).

| Variation (%,K) | −20 | −10 | 10 | 20 |
|---|---|---|---|---|
| variable | −2 | −1 | 1 | 2 |
| | | $T_a$ (K) | | |
| $r_a$ | 0.67 | 0.32 | −0.33 | −0.68 |
| $R_n$−G | 0.71 | 0.35 | −0.36 | −0.72 |
| $T_0$ | −1.18 | −0.59 | 0.61 | 1.21 |
| $\beta$ | 0.50 | 0.24 | −0.23 | −0.44 |

**Table 5.** The sensitivity of $e_a$ estimates from the ADEBAV method to each input variable. Variations of $T_a$ are in K, and variations of other variables are a percentage (%).

| Variation (%,K) | −20 | −10 | 10 | 20 |
|---|---|---|---|---|
| variable | −2 | −1 | 1 | 2 |
| | | $e_a$ (hpa) | | |
| $r_a$ | 0.43 | 0.22 | −0.21 | −0.43 |
| $r_s$ | 0.46 | 0.23 | −0.22 | −0.47 |
| $R_n$−G | 0.76 | 0.38 | −0.37 | −0.76 |
| $T_a$ | −0.19 | −0.10 | 0.11 | 0.22 |
| $\beta$ | −0.37 | −0.19 | 0.20 | 0.41 |

## 6. Conclusions

Radiation conditions, local meteorological conditions and land surface properties are the primary local factors determining near-surface air temperature and vapor pressure. Horizontal advection is the

exotic factor determining them. In the study, by considering the effects of the local driving force and horizontal advection on $T_a$ and $e_a$, methods for estimating $T_a$ and $e_a$ on a regional scale were proposed on the basis of the linear mixing theory. The energy balance equation was used to deduce the air temperature and the air vapor pressure in the condition of no horizontal advection. The measurements of wind speed, wind direction, $T_a$ and $e_a$ at weather stations were used to determine $T_a$ and $e_a$ affected by horizontal advection. One important assumption for the method proposed in the paper is that there is a similar horizontal advection in the pixel to be interpolated and the searched nearest two weather stations. Because horizontal advection usually has a similar effect at a regional scale, this assumption is reasonable. For example, similar wind speed can be observed within even several dozen kilometers in windy weather

Twenty weather stations were used in the study to perform the calculations of the ADEBAT/ADEBAV method, and another 20 weather stations were used to validate the method. The IDW method was also used to estimate the distributions of $T_a$ and $e_a$ and was compared with the methods presented in the paper. The results show that the accuracy of $T_a$ and $e_a$ estimates from the ADEBAT/ADEBAV method is much greater than that from the IDW method. $R^2$ between $T_a$ estimates from the ADEBAT method and $T_a$ measurements at weather stations are 0.77, 0.82 and 0.80 for the three days, while $R^2$ for the IDW method are only 0.3, 0.50 and 0.25. RMSE for the ADEBAT method are 0.42K, 0.35K and 0.2K, while for the IDW method 0.82K, 0.39K and 0.65K. Similar results were also observed for the ADEBAV method and for the IDW method. The ADEBAV method obtained better values of $R^2$ and RMSE. The values of $R^2$ are 0.85, 0.88, 0.88, and the RMSE values are 0.24hpa, 0.35hpa and 0.16hpa, respectively, for the three days; while for the IDW method, $R^2$ values are only 0.22, 0.33 and 0.03 and RMSE values 1.45hpa, 0.96hpa and 0.45hpa.

The advantage of the ADEBAT/ADEBAV method is that it takes into account the effects of not only horizontal advection, but also the local driving force on the near-surface atmosphere. While the IDW method only considers some effects of horizontal advection by calculating the distance of the pixel to be interpolated to the weather stations. The comparisons between the estimates of $T_a$ and $e_a$ from the ADEBAT/ADEBAV method and from the IDW method at Doping Lake proved this. The absolute biases between $T_a/e_a$ estimates from the ADEBAT method and $T_a/e_a$ measurements at the weather station of Doping Lake are 0.19K, 0.42K and 0.35K (0.5hpa, 0.7hpa and 0.6hpa), respectively, for the three days. Comparatively, the absolute biases between $T_a/e_a$ estimates from the IDW method and $T_a/e_a$ measurements are 4.33K, 2.36K and 3.33K (4.87hpa, 3.78hpa and 5.13hpa).

The results of the sensitivity analysis show that the ADEBAT method is sensitive most to surface temperature. A 1K increase of surface temperature could result in a 0.6K increase in $T_a$ estimates. The ADEBAV method is most sensitive to $R_n-G$. A 10% increase of $R_n-G$ could result in a 0.37-hpa decrease of $e_a$ estimates. As is known, the Bowen ration is difficult to estimate at a regional scale. However, the two methods are not very sensitive to it.

## Acknowledgments

This work was supported jointly by the National Basic Research Program of China (2013CB733406), the National Natural Science Foundation of China (41271380, 41171286) and the Open Fund of State Key Laboratory of Remote Sensing Science (OFSLRSS201510).

## Author Contributions

Renhua Zhang conceived and designed the research. Renhua Zhang, Yuan Rong and Jing Tian wrote the manuscript with the contributions from all co-authors and were responsible for the research design, data preparation and analysis. Hongbo Su and Zhaoliang Li provided some useful advices for the research and gave a lot of help in English writing. Suhua Liu gave some help in image processing.

## Conflicts of Interest

The authors declare no conflict of interest.

## References

1. Prihodko, L.; Goward, S.N. Estimation of air temperature from remotely sensed surface observations. *Remote Sens. Environ.* **1997**, *60*, 335–346.
2. Stisen, S.; Sandholt, I.; Norgaard, A.; Fensholt, R.; Eklundh, L. Estimation of diurnal air temperature using MSG SEVIRI data in West Africa. *Remote Sens. Environ.* **2007**, *110*, 262–274.
3. Li, J.; Heap, A.D. A review of comparative studies of spatial interpolation methods in environmental sciences: Performance and impact factors. *Ecol. Inform.* **2011**, *6*, 228–241.
4. Xu, C.D.; Wang, J.F.; Hu, M.G.; Li, Q.X. Interpolation of missing temperature data at meteorological stations using P-BSHADE. *J. Clim.* **2013**, *26*, 7452–7463.
5. Eldrandaly, K.A.; Abu-Zaid, M.S. Comparison of six GIS-based spatial interpolation methods for estimating air temperature in western Saudi Arabia. *J. Environ. Inform.* **2011**, *18*, 38–45.
6. Lennon, J.J.; Turner, J.R.G. Predicting the spatial distribution of climate: Temperature in Great Britain. *J. Anim. Ecol.* **1995**, *64*, 370−392.
7. Zhao, C.Y.; Nan, Z.R.; Cheng, G.D. Methods for modelling of temporal and spatial distribution of air temperature at landscape scale in the southern Qilian mountains, China. *Ecol. Model.* **2005**, *189*, 209−220.
8. You, J.S.; Hubbarda, K.G.; Goddard, S. Comparison of methods for spatially estimating stationtemperatures in a quality control system. *Int. J. Climatol.* **2008**, *28*, 777–787.
9. Dodson, R; Marks, D. Daily air temperature interpolated at highspatial resolution over a large mountainous region. *Clim. Res.* **1997**, *8*, 1–20.
10. Stahl, K.; Moore, R.D.; Floyer, J.A.; Asplin, M.G.; McKendry, I.G. Comparison of approaches for spatial interpolation of daily air temperature in a large region with complex topography and highly variable station density. *Agric. For. Meteorol.* **2006**, *139*, 224–236.
11. Benali, A.; Carvalho, A.C.; Nunes, J.P.; Carvalhais, N.; Santos, A. Estimating air surface temperature in Portugal using MODIS LST data. *Remote Sens. Environ.* **2012**, *124*, 108–121.
12. Mostovoy, G.V.; King, R.L.; Reddy, K.R.; Kakani, V.G.; Filippova, M.G. Statistical estimation of daily maximum and minimum air temperatures from MODIS LST data over the state of Mississippi. *GISci. Remote Sens.* **2006**, *43*, 78−110.
13. Vancutsem, C.; Ceccato, P.; Dinku, T.; Dinku, T.; Connor, S.J. Evaluation of MODIS land surface temperature data to estimate air temperature in different ecosystems over Africa. *Remote Sens. Environ.* **2010**, *114*, 449−465.

14. Zhu, W.B.; Lű, A.F.; Jia, S.F. Estimation of daily maximum and minimum air temperature using MODIS land surface temperature products. *Remote Sens. Environ.* **2013**, *130*, 62−73.
15. Goetz, S.J.; Prince, S.D.; Small, J. Advances in satellite remote sensing of environmental variables for epidemiological applications. *Adv. Parasitol.* **2000**, *47*, 289−307.
16. Shamir, E.; Georgakakos K.P. MODIS land surface temperature as an index of surface air temperature for operational snowpack estimation. *Remote Sens. Environ.* **2014**, *152*, 83−98.
17. Pape, R.; Löffler, J. Modelling spatio-temporal near-surface temperature variation in high mountain landscapes. *Ecol. Model.* **2004**, *178*, 483−501.
18. Sun, Y.J.; Wang, J.F.; Zhang, R.H.; Gillies, R.R.; Xue, Y.; Bo, Y.C. Air temperature retrieval from remote sensing data based on thermodynamics. *Theor. Appl. Climatol.* **2005**, *80*, 37−48.
19. Prince, S.D.; Goetz, S.J.; Dubayah, R.O.; Czajkowski, K.P.; Thawley, M. Inference of surface and air temperature; atmospheric precipitable water andvapor pressure deficit using advanced very high-resolution radiometer satelliteobservations: Comparison with field observations. *J. Hydrol.* **1998**, *212*, 230−249.
20. Wilson, K.; Goldstein, A.; Falge, E.; Aubinet, M.; Baldocchi, D.; Berbigier, P.; Bernhofer, C.; Ceulemans, R.; Dolman, H.; Field, C.; *et al.* Energy balance closure at FLUXNET sites. *Agric. For. Meteorol.* **2002**, *113*, 223–243.
21. Granger, R.J. Satellite-derived estimates of evapotranspiration in the Gediz basin. *J. Hydrol.* **2000**, *229*, 70−76.
22. Hashimoto, H. ; Dungan, J.L.; White, M.A.; Yang, F.H.; Michaelisa, A.R.; Running, S.W.; Nemani,R.R. Satellite-based estimation of surface vapor pressure deficitsusing MODIS land surface temperature data. *Remote Sens. Environ.* **2008**, *112*, 142–155.
23. Sobrino, J A.; Kharraz, J.E. Surface temperature and water vapor retrieval from MODIS data. *Int. J. Remote Sens.* **2003**, *24*, 5161–5182.
24. Recondo, C.; Pendás, E.; Moreno, S.; de Vicuña, C.G.; García-Martínez, A.; Abajo, A.; Zapico, E. A simple empirical method for estimating surface water vapour pressure using MODIS near-infrared channels: Applications to northern Spain's Asturias region. *Int. J. Remote Sens.* **2013**, *34*, 3248–3273
25. Tian, J.; Zhang, R.H.; Sun, X.M.; Zhu, Z.L.; Zhou, Y.L. Study of a model for correcting the effects of horizontal advection on surface fluxes measurement based on remote sensing. *Sci. China Ser. D: Earth Sci.* **2006**, *49*, 273–280.
26. Yang, Y.M.; Su, H.B.; Zhang, R.H.; Xia, J. Revised advection-aridity evaporation model. *J. Hydrol. Eng.* **2012**, *18*, 655–664.
27. Bastiaanssen, W.G.M.; Menenti, M.; Feddes, R.A.; Holtslag, A.A.M. A remote sensing surface energy balance algorithm for land (SEBAL) 1. Formulation. *J. Hydrol.* **1998**, *212*, 198–212.
28. Su, Z.B. The surface energy balance system (SEBS) for estimation of turbulent heat fluxes. *Hydrol. Earth Sys. Sci.* **2002**, *6*, 85–89.
29. Boegh, E.; Soegaard, H.; Thomsen, A. Evaluating evapotranspiration rates and surface conditions using Landsat TM to estimate atmospheric resistance and surface resistance. *Remote Sens. Environ.* **2002**, *79*, 329–343.
30. Wang, K.C; Dickinson, R.E. A review of global terrestrial evapotranspiration : Observation, modelling, climatology, and climatic variablility. *Rev. Geophys.* **2012**, *50*, 1–54.

31. Zhang, R.H.; Sun, X.M.; Zhu, Z.L.; Su, H.B.; Tang, X.Z. A remote sensing model for monitoring soil evaporation based on differential thermal inertia and its validation. *Sci. China Ser. D: Earth Sci.* **2003**, *46*, 342–356.
32. Zhang, R.H.; Tian, J.; Su, H.B.; Sun, X.M.; Chen, S.H.; Xia, J. Two improvements of an operational two-layer model for terrestrial surface heat flux retrieval. *Sensors* **2008**, *8*, 6165–6187.
33. Moran, M.S.; Clarke, T.R.; Inoue, Y.; Vidal, A. Estimating crop water deficit using the relation between surface-air temperature and spectral vegetation index. *Remote Sens. Environ.* **1994**, *49*, 246–263.
34. Jiang, L.; Islam, S. Estimation of surface evaporation map over southern Great Plains using remote sensing data. *Water Resour. Res.* **2001**, *37*, 329–340.
35. Nishida, K.; Namani, R.R.; Running, S.W.; Glassy, J.M. An operational remote sensing algorithm of land surface evaporation. *J. Geophys. Res.* **2003**, *108*, 42–70.
36. Carlson, T. An overview of the "Triangle Method" for estimating surface evapotranspiration and soil moisture from satellite imagery. *Sensors* **2007**, *7*, 1612–1629.
37. Chen, C.; Wang, E.L.; Yu, Q. Modeling wheat and maize productivity as affacted by climate variation and irrigation supply in North China Plain. *Agron. J.* **2010**, *102*, 1037–1049.
38. Wu, D.R.; Yu, Q.; Lu, C.H.; Hengsdijk, H. Quantifying production potentials of winter wheat in the North China Plain. *Eur. J. Agron.* **2006**, *24*, 226–235.
39. Camillo, P.J.; Gurney, R.J. A resistance parameter for bare soil evaporation models. *Soil Sci.* **1986**, *141*, 95–105.
40. Sun, S.F. Moisture and Heat Transport in A Soil Layer Forced by Atmospheric Conditions. Master's Thesis, University of Connecticut, Mansfield, CT, USA, 1982.
41. Qin, Z.; Karnieli, A.; Berliner, P. A mono-window algorithm for retrieving land surface temperature from Landsat TM data and its application to the Israel-Egypt border region. *Int. J. Remote Sens.* **2001**, *22*, 3719–3746.
42. Liang, S.L. Narrowband to broadband conversions of land surface albedo I: Algorithms. *Remote Sens. Environ.* **2000**, *76*, 213–238.
43. Tang, B.H.; Bi, Y.Y.; Li, Z.L.; Xia, J. Generalized split-window algorithm for estimate of land surface temperature from Chinese geostationary FengYun meteorological satellite (FY-2C) data. *Sensors* **2008**, *8*, 933–951.